Conference Paper, Published Version

Kim, Tae Boem; Yang, Jeong-Seok

Numerical Modeling of Flow in Curved Channels with Various Sinuousness

ICHE 2014, Hamburg - Lehfeldt & Kopmann (eds) - © 2014 Bundesanstalt für Wasserbau ISBN 978-3-939230-32-8

Numerical Modeling of Flow in Curved Channels with Various Sinuousness

T.B. Kim & J.-S. Yang
School of Civil and Environmental Engineering, Kookmin University, Seoul, Korea

ABSTRACT: It is well known that the flow in curved channels is much more complex than the straight channel. Due to the centrifugal force, the helicoidal flow (sometimes, this is called as the secondary current in curved channels) and super-elevation of water surface are induced in curved channels. In order to simulate such complex flows, 3D numerical model is required. However, 2D numerical model is favorably chosen by practical engineers because of relative simplicity in implementation and application compared to 3D model. The purpose of this study is 2D numerical modeling of open-channel flow in bends in order to investigate the influence of channel sinuousness and flow discharge on flow characteristics. The depth-averaged Reynolds equation and finite element method are adopted as governing equation and numerical method for 2D numerical flow model. All of conditions or parameters given through experiments in sine-generated curved channel with 30°, 60°, and 110° maximum deflection angles are applied identically to numerical model. The results of flow characteristics depending on the flow discharge and channel sinuousness are analyzed.

Keywords: Meandering, Curved channel, Numerical model

1 INTRODUCTION

Meandering river rather than the straight can be commonly seen in the nature. Therefore, various phenomena occurred in curved channels have been important and interesting topics over the last several decades. Through a lot of researches, it is well known that the flow in curved channels is much more complex than the straight channel. Due to the centrifugal force, the helicoidal flow (sometimes, this is called as the secondary current in curved channels) and super-elevation of water surface are induced in curved channels. Due to these flow characteristics in curved channels, point bar and pool are created near the inner bank and the outer bank, respectively, and the bank erosion is threatened by the wall shear stress. In spite of a lot of researches for decades, many fundamental mechanisms and interrelationships between geometry and flow conditions are remained as the undiscovered and challenged category.

To investigate the flow characteristics and turbulent structure in curved channels, laboratory experiments have been conducted in recent years by several researchers (Liu et al., 2005; da Silva et al., 2006; Abad and Garcia, 2009; Blanckaert, 2009; Termini and Piraino, 2011). However, most of these experiments were carried out in one or two specific shaped channel, because physical models have restrictions on time, space, scale, and costs in their operation and practice. These restrictions make detailed and intensive investigation and further research on flow structure and interrelationship between channel geometry and flow conditions difficult.

Therefore, in this study, alternatively numerical model is applied to investigate the flow structure in curved channels. In order to simulate such complex flows in curved channels, 3D numerical model is required. However, 2D numerical model is favorably chosen by practical engineers because of relative simplicity in implementation and application compared to 3D model. The effects of channel sinuousness and flow discharge on flow structure is investigated with 2D numerical open-channel flow model.

2 GOVERNING EQUATIONS AND NUMERICAL METHOD

2.1 *Governing Equations*

The following depth-averaged Reynolds equations are adopted as the governing equations for 2D flow model.

$$\frac{\partial h}{\partial t}+\frac{\partial p}{\partial x}+\frac{\partial q}{\partial y}=0 \tag{1}$$

$$\frac{\partial p}{\partial t}+\frac{\partial}{\partial x}\left(\frac{p^2}{h}+\frac{gh^2}{2}\right)+\frac{\partial}{\partial y}\left(\frac{pq}{h}\right)-\frac{\partial}{\partial x}\left(2\nu_t\frac{\partial p}{\partial x}\right)-\frac{\partial}{\partial y}\left[\nu_t\left(\frac{\partial p}{\partial y}+\frac{\partial q}{\partial x}\right)\right]+gh\frac{\partial z_b}{\partial x}+\frac{1}{\rho}\tau_{bx}=0 \tag{2}$$

$$\frac{\partial q}{\partial t}+\frac{\partial}{\partial x}\left(\frac{pq}{h}\right)+\frac{\partial}{\partial y}\left(\frac{q^2}{h}+\frac{gh^2}{2}\right)-\frac{\partial}{\partial x}\left[\nu_t\left(\frac{\partial p}{\partial y}+\frac{\partial q}{\partial x}\right)\right]-\frac{\partial}{\partial y}\left(2\nu_t\frac{\partial q}{\partial y}\right)+gh\frac{\partial z_b}{\partial y}+\frac{1}{\rho}\tau_{by}=0 \tag{3}$$

where h = water depth, p and q = unit discharges in the x- and y-directions, respectively, g = gravity acceleration, ν_t = turbulent viscosity, z_b = channel bed elevation, ρ = fluid density, and τ_{bx} and τ_{by} = x- and y-components of the bed shear stress, respectively. The x- and y-components of depth-averaged velocity, u and v, can be estimated with the relationship of $u = p/h$ and $v = q/h$, respectively.

τ_{bx} and τ_{by} are given by applying the Manning's equation as the followings:

$$\tau_{bx}=\frac{\rho g n^2}{h^{7/3}}p\left(p^2+q^2\right)^{1/2},\quad \tau_{by}=\frac{\rho g n^2}{h^{7/3}}q\left(p^2+q^2\right)^{1/2} \tag{4}$$

where n = Manning's roughness coefficient.

The following relationship for turbulent viscosity is adopted.

$$\nu_t=\frac{\kappa}{6}U_* h \tag{5}$$

where κ = von Kármán's constant (≈ 0.41) and U_* = shear velocity.

2.2 *Numerical Method*

To obtain the numerical solution for the open-channel flows, the finite element method is adopted in this study. The weighted residual equation of Eqs. (1) ~ (3) for FEM is as the following:

$$\int_\Omega N^*\left(\frac{\partial \mathbf{U}}{\partial t}+\mathbf{A}\frac{\partial \mathbf{U}}{\partial x}+\mathbf{B}\frac{\partial \mathbf{U}}{\partial y}+\frac{\partial \mathbf{D_x}}{\partial x}+\frac{\partial \mathbf{D_y}}{\partial y}+\mathbf{F}\right)d\Omega=0 \tag{6}$$

where Ω = model domain, and N^* = weighting function. The terms of Eq. (6) enclosed in the brackets represent a matrix form of governing equation, in which **U** is the solution vector, **A** and **B** the convection matrices, $\mathbf{D_x}$ and $\mathbf{D_y}$ the turbulent diffusion vectors, and **F** the force vector playing a role as a source.

Depending on the weighting function, a various finite element schemes are introduced. In this study, SU/PG scheme showing the following weighting function is employed.

$$N_i^*=N_i+\omega\Delta x\frac{\partial N_i}{\partial x}\mathbf{W_x}+\omega\Delta y\frac{\partial N_i}{\partial y}\mathbf{W_y} \tag{7}$$

where N_i^* and N_i = weighting and basis functions for the i-th node, respectively, ω = weighting coefficient, and $\mathbf{W_x}$ and $\mathbf{W_y}$ = weighting matrices in the x- and y-directions, respectively, which are suggested by Ghanem (1995) as the following:

$$\mathbf{W_x}=\frac{\mathbf{A}}{\sqrt{\mathbf{A}^2+\mathbf{B}^2}},\quad \mathbf{W_y}=\frac{\mathbf{B}}{\sqrt{\mathbf{A}^2+\mathbf{B}^2}} \tag{8}$$

Δx and Δy in Eq. (7) are estimated as the following which is suggested by Katopodes (1984):

$$\Delta x = 2\sqrt{\left(\frac{\partial x}{\partial \xi}\right)^2 + \left(\frac{\partial x}{\partial \eta}\right)^2},\ \Delta y = 2\sqrt{\left(\frac{\partial y}{\partial \xi}\right)^2 + \left(\frac{\partial y}{\partial \eta}\right)^2} \tag{9}$$

where ξ and η = local coordinates.

Eq. (6) is applied to all elements within the modeled area. Then, nonlinear equations are obtained, which are linearized by using the Newton-Raphson method. Through solving the linear matrix system, the numerical solution for 2D open-channel flow can be obtained.

3 APPLICATION

Xu and Bai (2013) conducted series of experiments with physical models in a small scale. The water was circulated with a pump and pipe from a tank at tail to channel head. The water discharge was controlled with a ball valve and measured at tail. The channel was filled with non-uniform sand with a mean grain size of 0.73 mm. The shape of channels were made as sine-generated with river bank by driving organic plastic sheets into the bed. The centerlines of channel followed a sine-generated curve as the following:

$$\theta = \theta_0 \sin\left(2\pi \frac{s}{L}\right) \tag{10}$$

where θ = deflection angle at any point following the centerline of channel, θ_0 = maximum deflection angle, s = longitudinal coordinate along the centerline of channel, and L = longitudinal wavelength. Xu and Bai (2013) conducted totally 8 experimental run with the combination of channel sinuosness and water discharge. The geometric and hydraulic conditions of 6 experimental runs which were chosen in this study are listed in Table 1.

Table 1. Geometric and hydraulic characteristics in experiments of Xu and Bai (2013)

Max. deflection angle (θ_0)	Longitudinal wavelength (L)	Discharge [m^3/s]	Mean depth of water [m]	Mean flow velocity [m/s]	Froude number	Manning's roughness (n)
30°	1.0	0.68×10^{-3}	0.0151	0.30	0.78	0.0110
		1.55×10^{-3}	0.0344	0.30	0.52	0.0193
60°	2.0	0.68×10^{-3}	0.0227	0.20	0.42	0.0220
		1.55×10^{-3}	0.0413	0.25	0.39	0.0262
110°	2.5	0.68×10^{-3}	0.0252	0.18	0.36	0.0262
		1.55×10^{-3}	0.0470	0.22	0.32	0.0324

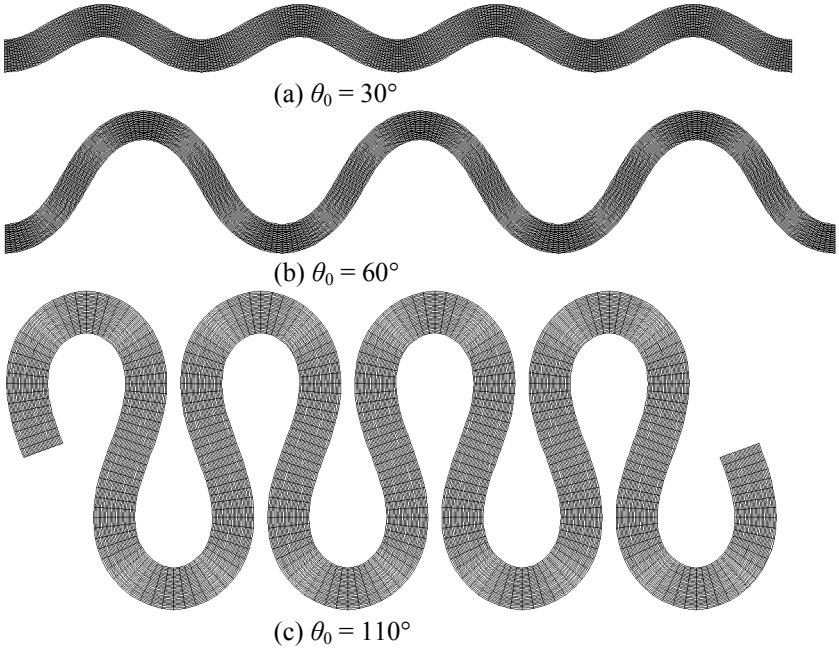

(a) $\theta_0 = 30°$

(b) $\theta_0 = 60°$

(c) $\theta_0 = 110°$

Figure 1. Geography of sine-generated channel for numerical modeling

Channel width and bed slope are 0.15 m and 0.003, respectively, which are identical in all experiments. All of conditions or parameters given through experiments of Xu and Bai (2013) were applied identically

to numerical model. It is noted that Manning's roughness coefficients in the last column of Table 1 were estimated for numerical modeling based on the hydraulic data given at Xu and Bai (2013), because they did not clearly describe the roughness of channel bed. It can be known through these estimation that depending on the physical model scale the extent and effect of channel roughness can be changed, although bed material and geometry of channel are same.

By using Eq. (10), totally 3 kinds of finite element meshes with linear quadrilateral elements were made up as shown in Figure 1. When the maximum deflection angles were 30° and 110°, 4 periods of sine-generated curves were used as shown in Figures 1(a) and 1(c), resulting in 9,951 nodes and 9,600 elements composed. When the maximum deflection angle was 60°, 3 periods of sine-generated curves were used as shown in Figure 1(b), resulting in 7,471 nodes and 7,200 elements composed. Because experiments in laboratory were conducted within the basin with the length of 4 m, these difference of periods was induced.

Figures 2 and 3 show the comparison of calculated velocity vectors along cross-sections with observation. Both of calculated and observed flow velocity distribution have such a same trend that velocity near convex bank at a streamwise position is higher than that near concave bank and the maximum flow velocity shifts to the opposite bank from one apex to the next apex. However, flow detachment near the convex bank just downstream of the apex and reattachment near the concave bank just upstream of the next apex are observed in experimental results as shown in Figures 2(a) and 3(a) whilst in calculated results the highest velocity on a cross-section near the convex bank just downstream of the apex is maintained as shown in Figures 2(b) and 3(b). This is due to the difference of obtained data type. The flow velocities obtained with numerical model represent values of depth-averaged field, while observed velocities represent those of surface flow field which were measured with particle tracking velocimeter composed with scattered seeding particles, camera, and analyzing computer program. In curved channels, bulk of fluid elements is pushed outward from near convex bank toward near concave bank by centrifugal force. Due to the flow resistance near the bed, fluid elements near the water surface can move outward freely in relative, resulting in the occurrence of super-elevation phenomena. Therefore, it can be inferred that low velocity area near the convex bank just downstream of the apex observed in experiments is just due to tracing lines of suspending particles on water surface which reflect predominant centrifugal force. Pressure increase near the concave bank due to the super-elevation and compensation for the loss of fluid mass near the convex bank cause the fluid elements shifted along near channel bed from concave bank toward convex bank. Therefore, it can be considered that low velocity area as observed in experiment cannot be caught in numerical model, because outward component near water surface and inward component near channel bed are depth-averaged and cancelled each other.

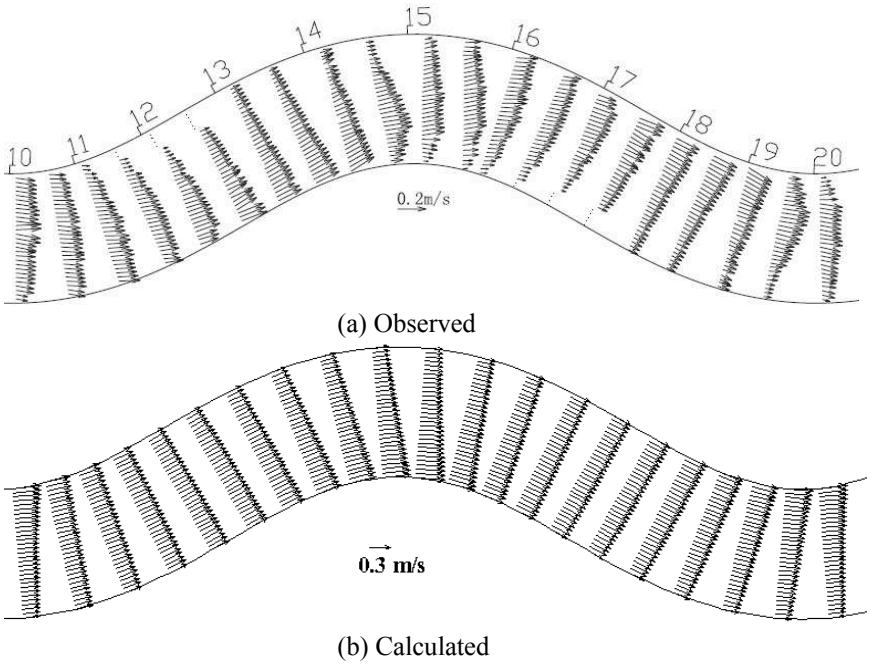

(a) Observed

(b) Calculated

Figure 2. Velocity vectors in channel of $\theta_0 = 30°$

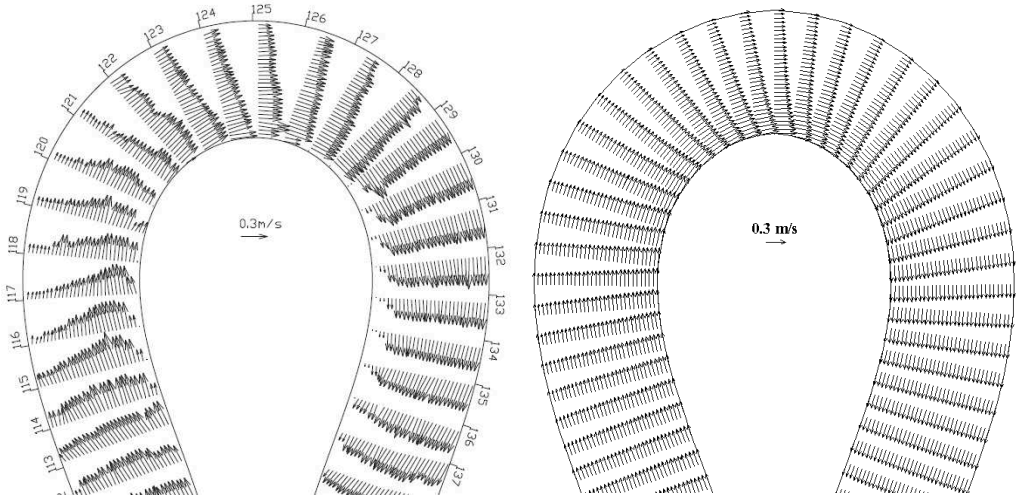

(a) Observed (b) Calculated

Figure 3. Velocity vectors in channel of $\theta_0 = 110°$

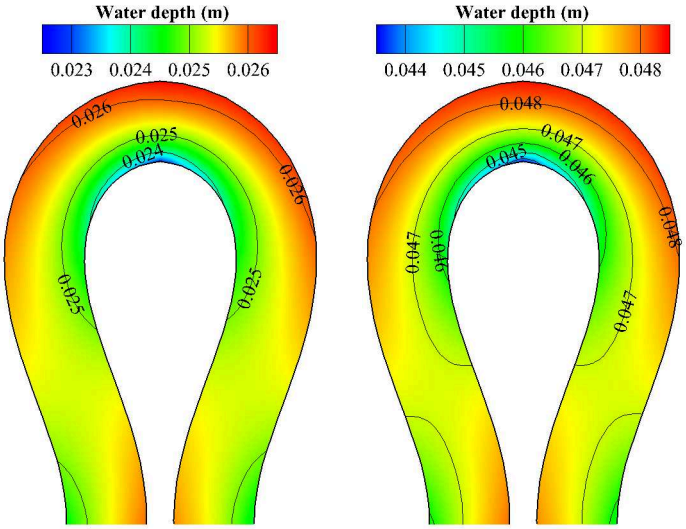

(a) $Q = 0.68 \times 10^{-3}$ m^3/s (b) $Q = 1.55 \times 10^{-3}$ m^3/s

Figure 4. Distribution of water depth in channel of $\theta_0 = 110°$

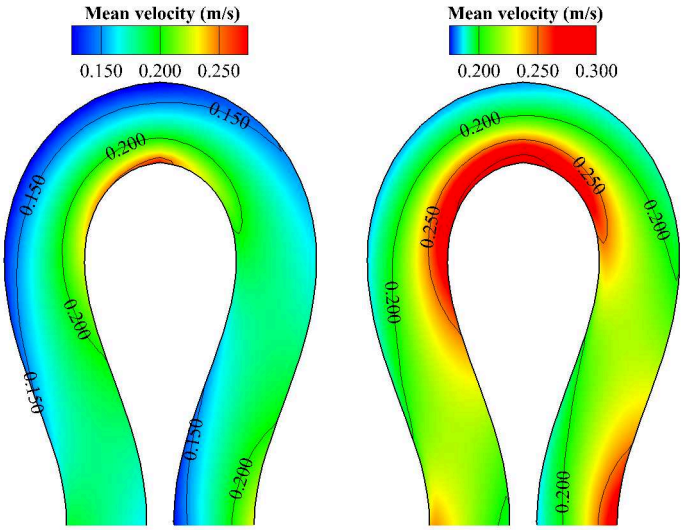

(a) $Q = 0.68 \times 10^{-3}$ m^3/s (b) $Q = 1.55 \times 10^{-3}$ m^3/s

Figure 5. Distribution of mean velocity in channel of $\theta_0 = 110°$

Figures 4 and 5 show the calculated results of the distribution of water depth and mean velocity, respectively, in channel bends of 110° maximum deflection angle depending on the flow discharge. These show

a typical feature of curved channel flow on which the water depth near the concave bank is deeper than that near the convex bank and the flow velocity near the convex bank is higher than that near the concave bank. In addition, it is shown that as the water discharge increases, transitional area of water depth and flow velocity along around the convex and concave banks also increases.

Figure 6 shows the cross-sectional distribution of water depth at apex normalized with the mean depth of water (h_0) corresponding to the fourth column in Table 1. A horizontal axis represents the distance from the centerline of channel. Left side having negative values shows the approach to concave bank and right side vice versa. In Figure 6, super-elevation phenomena can be definitely observed. In addition, it is interestingly observed that as flow discharge increases, the rate of change in water depth decreases. In general thinking, increase of flow discharge resulting in increase of flow velocity causes the rate of change in water depth around channel bends increase. However, the calculated results show exactly the opposite of what it is expected. It may be considered that increase of flow discharge causes the water depth increase. As a result, gravitational force acts relatively stronger to increased volume of water and advection of flow tends to dominate. Therefore, the incline of water depth with respect to mean water depth is less than that of small flow discharge. Additionally, as the maximum deflection angle increases, the junction point where the water depth coincides with the mean value is shifted toward convex bank.

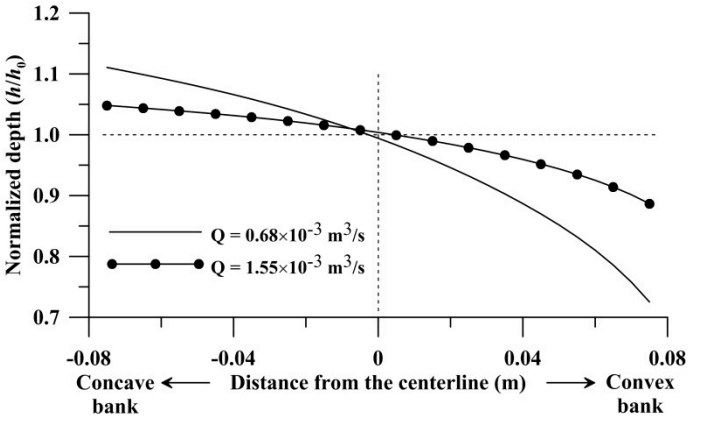

(a) $\theta_0 = 30°$

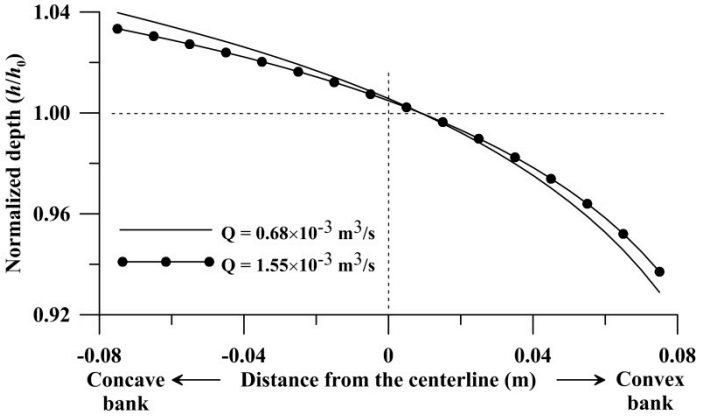

(b) $\theta_0 = 60°$

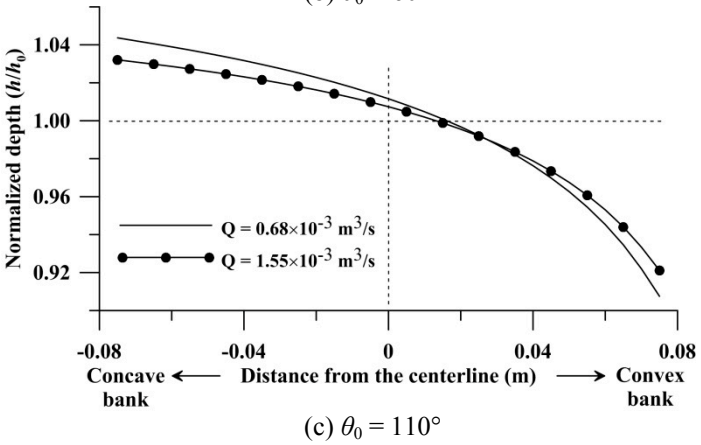

(c) $\theta_0 = 110°$

Figure 6. Cross-sectional distribution of normalized water depth at apex

4 CONCLUSIONS

In this study, 2D finite element numerical model for open-channel flows was applied to 3 types of sine-generated curved channel which correspond to 30°, 60°, and 110°, respectively. In each sine-generated curved channels, 2 kinds of water discharge were used as boundary conditions with identical width and slope of channel. The calculated results showed such a typical trend of curved open-channel flows that velocity and water depth near convex bank were higher and shallower, respectively, than those near concave bank and the maximum flow velocity shifted to the opposite bank from one apex to the next apex. However, low velocity area as observed in experiment could not be caught in numerical model, because outward component near water surface and inward component near channel bed were depth-averaged and cancelled each other.

It can be known through numerical modeling that transitional area of water depth and flow velocity along around the convex and concave banks increases and the rate of change in water depth with respective to mean water depth at apex decreases as the flow discharge increases, and that the junction point where the water depth coincides with the mean water depth is shifted toward convex bank as the maximum deflection angle increases.

ACKNOWLEDGMENTS

This research was supported by Basic Science Research Program through the National Research Foundation of Korea (NRF) funded by the Ministry of Education (grant no. 2013R1A1A2060622).

NOTATION

η	local coordinate in finite element mesh
κ	von Kármán's constant (≈ 0.41)
ν_t	turbulent viscosity
θ	deflection angle at any point of sine-generated curve
θ_0	maximum deflection angle of sine-generated curve
ρ	fluid density
τ_{bx}	x-component of bed shear stress
τ_{by}	y-component of bed shear stress
ω	weighting coefficient in SU/PG scheme
ξ	local coordinate in finite element mesh
Ω	model domain
g	gravity acceleration
h	depth of water
h_0	mean depth of water
L	longitudinal wavelength of sine-generated curve
N	basis function of finite element method
N^*	weighting function of finite element method
n	Manning's roughness coefficient
p	x-component of unit discharge
Q	flow discharge
q	y-component of unit discharge
s	longitudinal coordinate of sine-generated curve
U_*	shear velocity
u	x-component of depth-averaged velocity
v	y-component of depth-averaged velocity
Δx	length of finite element mesh in x-direction
Δy	length of finite element mesh in y-direction
z_b	bed elevation
$\mathbf{A}$	convection matrix in matrix form of governing equations
$\mathbf{B}$	convection matrix in matrix form of governing equations
$\mathbf{D_x}$	turbulent diffusion vector in matrix form of governing equations
$\mathbf{D_y}$	turbulent diffusion vector in matrix form of governing equations
$\mathbf{F}$	source vector in matrix form of governing equations
$\mathbf{U}$	solution vector in matrix form of governing equations
$\mathbf{W_x}$	weighting matrix in x-direction of SU/PG scheme
$\mathbf{W_y}$	weighting matrix in y-direction of SU/PG scheme

REFERENCES

Abad, J.D., Garcia, M.H. (2009). Experiments in a high-amplitude Kinoshita meandering channel: 1. Implications of bend orientation on mean and turbulent flow structure. Water Resources Research, Vol. 45, W02401.

Blanckaert, K. (2009). Saturation of curvature-induced secondary flow, energy losses, and turbulence in sharp open-channel bends: laboratory experiments, analysis, and modeling. Journal of Geophysical Research, Vol. 114, F03015.

da Silva, A.M.F., El-Tahawy, T., Tape, W.D. (2006). Variation of flow pattern with sinuosity in sine-generated meandering streams. Journal of Hydraulic Engineering, Vol. 132, No. 10, pp. 1003-1014.

Ghanem, A.H.M. (1995). Two-dimensional finite element modeling of flow in aquatic habitats. Ph.D. Thesis, University of Alberta, Alberta.

Katopodes, N.D. (1984). Two-dimensional surges and shocks in open channels. Journal of Hydraulic Engineering, Vol. 110, No. 6, pp. 794-812.

Liu, Y.Q., Zheng, S.W., Wu, Q. (2005). Experimental study of 3-D turbulent bend flows in open channel. Journal of hydrodynamics, Vol. 17, pp. 704-712.

Termini, D., Piraino, M. (2011). Experimental analysis of cross-sectional flow motion in a large amplitude meandering bend. Earth Surface Processes and Landforms, Vol. 36, No. 2, pp. 244-256.

Xu, D., Bai, Y. (2013). Experimental study on the bed topography evolution in alluvial meandering rivers with various sinuousnesses. Journal of Hydro-environment Research, Vol. 7, No.2, pp. 92-102